



Provided for non-commercial research and education use.
Not for reproduction, distribution or commercial use.



Volume 404, Issues 23–24, 15 December 2009 ISSN 0921-4526

PHYSICA **B**
CONDENSED MATTER
Recognized by the European Physical Society




Proceedings of the 25th International
Conference on Defects in Semiconductors

ICDS-25

held in Saint Petersburg, Russia
20–24 July 2009

Guest Editors:
N.T. Bagraev
V.V. Emtsev
S.K. Estreicher

Available online at www.sciencedirect.com <http://www.elsevier.com/locate/physb>

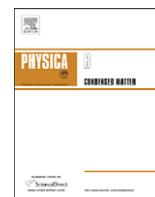
 ScienceDirect

This article appeared in a journal published by Elsevier. The attached copy is furnished to the author for internal non-commercial research and education use, including for instruction at the authors institution and sharing with colleagues.

Other uses, including reproduction and distribution, or selling or licensing copies, or posting to personal, institutional or third party websites are prohibited.

In most cases authors are permitted to post their version of the article (e.g. in Word or Tex form) to their personal website or institutional repository. Authors requiring further information regarding Elsevier's archiving and manuscript policies are encouraged to visit:

<http://www.elsevier.com/copyright>



X-ray diffraction on precipitates in Czochralski-grown silicon

O. Caha*, M. Meduňa

Department of Condensed Matter Physics, Masaryk University, Kotlářská 2, CZ-61137 Brno, Czech Republic

ARTICLE INFO

PACS:

61.72.Dd

61.72.Cc

61.72.uf

Keywords:

Silicon

X-ray diffraction

Precipitates

ABSTRACT

The results of a study of oxygen precipitates in Czochralski grown silicon are reported. High-resolution X-ray diffraction was used to measure reciprocal space maps on samples after various annealing treatment. The measurements were performed for several diffraction orders and systematic differences between reciprocal space maps around different diffractions were found. The diffuse X-ray scattering intensity was simulated, where the displacement field of precipitates was calculated using continuum elasticity theory. The simulations give correct asymptotic behavior and the interpretation of intermediate region between Huang and core scattering processes is found. The X-ray diffraction results are correlated to the infrared absorption spectroscopy measurement involving the interstitial oxygen concentration.

© 2009 Elsevier B.V. All rights reserved.

1. Introduction

Structural quality of semiconductor wafers and epitaxial layers is an important parameter substantially influencing their electrical properties and the performance of fabricated integrated circuits. A reliable control of the defect nucleation and growth during the semiconductor technology is an important issue, since the defects may affect detrimentally the electric parameters of the semiconductor structures. However, they can also be beneficial, since they can getter out impurities, especially heavy metal atoms. Silicon wafers pass through the series of thermal operations during the production technology of integrated circuits thus the oxygen precipitation plays an important role.

The X-ray methods and especially the diffuse scattering were used to study precipitates and other defects like dislocation loops for a long time [1–3]. The standard method for the precipitate radius determination is based on finding the point q_c where Huang scattering transforms into the core scattering [4]. Thus the X-ray precipitate radius is usually assumed to be $R_x = \pi/q_c$. However, this method gives the size of the precipitates in the crystal much larger than the size of the SiO_2 particle itself. The problems of this assumption were critically discussed by Larson [5]. In this paper we study the correspondence of the precipitate radius obtained by X-ray diffraction and with respect to the total volume of precipitates obtained by infrared absorption spectroscopy.

2. Experiment

The investigated samples were cut from low boron doped Czochralski grown silicon (111) wafer with a thickness of about 3 mm. The wafer came from the seed end of the ingot with the interstitial oxygen concentration of $7.3 \times 10^{17} \text{ cm}^{-3}$. The samples were annealed for 6 min at 1000 °C in order to dissolve the nuclei of precipitates formed during ingot pulling. The subsequent temperature process consisted of 24 h nucleation annealing at 600 °C and precipitation annealing at 800 °C up to 144 h. The series of six samples was prepared varying in the length of precipitation annealing. The precipitates nuclei were formed during the nucleation annealing stage at relatively high concentration of about $3 \times 10^{11} \text{ cm}^{-3}$. The precipitation annealing leads just to the growth of the nuclei and no new precipitates are formed. All the samples in the studied series have therefore the same precipitate concentration and only their size is increasing with the annealing time.

The reciprocal space maps (RSM) of X-ray scattered intensity were measured in symmetric (111), (333) and asymmetric (224) diffractions. The high resolution diffractometer with a conventional Cu X-ray tube was used. The beam optics consisted of a parabolic multilayer mirror and a Bartels-type monochromator. The signal was collected by a point detector with a channel-cut analyzer behind the sample. The detector was open in the direction perpendicular to the diffraction plane q_y and the measured intensity was therefore integrated along this direction.

An example of measured RSMs around (111) diffraction point on two samples is presented in Fig. 1. A crystal truncation rod perpendicular to sample surface and an analyzer streak along the detector scan induced by the dynamical diffraction effect from sample and analyzer crystal are evident in these RSMs. The

* Corresponding author. Tel.: +420 549493388; fax: +420 541211214.
E-mail address: caha@physics.muni.cz (O. Caha).

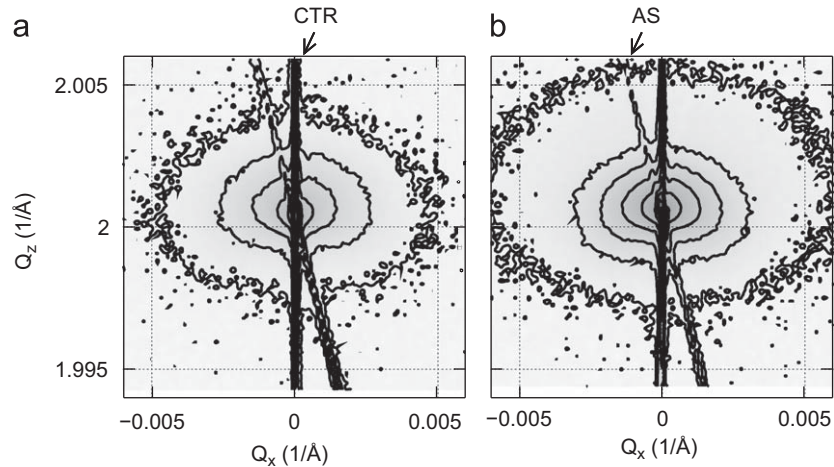


Fig. 1. Reciprocal space maps around (111) reciprocal lattice point of samples annealed for 48 h (a) and 144 h (b). The contour step is $10^{1/2}$. CTR denotes the crystal truncation rod and AS the analyzer streak.

remaining diffuse scattered intensity on precipitates is symmetrically distributed with respect to the Q_z -axis. Higher diffuse scattered intensity can be seen for the longer annealing time. The detailed analysis of the scattering is presented in Section 4.

The infrared (IR) absorption spectroscopy was performed on a Fourier transform Bruker IFS Equinox spectrometer in a spectral range from 400 to 6000 cm^{-1} at room and liquid nitrogen temperatures in order to distinguish between the absorption peak of interstitial silicon and SiO_x precipitates. The interstitial oxygen concentration was determined according to Ref. [6].

3. Theory of X-ray diffuse scattering

The amplitude of diffuse scattering can be written as a sum of core and Huang terms in the kinematical approximation [7]. The diffuse intensity can be then expressed as

$$I(\mathbf{q}) \sim \int |\Phi_C^{\text{FT}}(\mathbf{q}) + \Phi_H^{\text{FT}}(\mathbf{q})|^2 d\mathbf{q}_y, \quad (1)$$

where \mathbf{q} is reduced scattering vector defined as a difference of scattering vector and nearest reciprocal lattice vector $\mathbf{q} = \mathbf{Q} - \mathbf{h}$. The core term represents kinematical scattering on the nondiffracting precipitate core

$$\Phi_C(\mathbf{r}) = -\Omega(\mathbf{r})\chi_{\mathbf{h}}, \quad (2)$$

where $\Omega(\mathbf{r})$ is a shape function of the precipitate core and $\chi_{\mathbf{h}}$ is the \mathbf{h} -th component of susceptibility of the surrounding crystal. The core scattering is the leading term far from the reciprocal lattice point. Real precipitates always have nonuniform sizes; the averaged intensity from the core scattering decreases as q^{-4} [4]. Since our experimental setup integrates the intensity along q_y direction, the experimental intensity distribution decreases as q^{-3} .

The Huang scattering on the deformed lattice outside the precipitate core is given by the expression

$$\Phi_H(\mathbf{r}) = \tilde{\Omega}(\mathbf{r})\chi_{\mathbf{h}}[e^{-i\mathbf{h}\cdot\mathbf{u}(\mathbf{r})} - 1], \quad (3)$$

where $\tilde{\Omega}(\mathbf{r}) = 1 - \Omega(\mathbf{r})$ is the complementary shape function and $\mathbf{u}(\mathbf{r})$ is the displacement vector. The displacement was calculated as the convolution of the defect shape function and elastic Green function for the cubic crystal [8]. Efficient numerical solution is done in the Fourier space, where the convolution is a simple product of analytic functions [3,8]. Far from the precipitate the displacement field decreases as $u \sim r^{-2}$, though the displacement

depends on the crystallographic direction. In the elastically isotropic material the displacement outside the spherical precipitate is

$$u(\mathbf{r}) = \frac{pV}{4\pi r^2} = \frac{pR_c^3}{3r^2}, \quad (4)$$

where $V = 4/3\pi R_c^3$ is the volume of defect core, R_c is the radius of defect core and p is a deformation strength of the precipitate. The deformation strength p is defined as the ratio $p = \Delta V/V$, where ΔV is the difference of the real volume of the precipitate and the available volume in the unstrained silicon lattice. In the approximation of the small deformation $\mathbf{h} \cdot \mathbf{u} \ll 1$ we can expand the exponential in the Huang scattering term as

$$e^{-i\mathbf{h}\cdot\mathbf{u}(\mathbf{r})} - 1 \approx -i\mathbf{h} \cdot \mathbf{u}(\mathbf{r}). \quad (5)$$

Then such displacement dependence leads to the intensity distribution decreasing as q^{-2} . In our experimental setup the intensity decreases as q^{-1} due to suppressed resolution in the q_y direction.

4. Results and discussion

The analysis of the measured intensity distribution in the reciprocal space was done by analysis of the cuts performed along q_x direction. The cuts through the RSMs presented in Fig. 1 are shown in Fig. 2. We can clearly see the regions of Huang and core scattering, where the intensity depends on q as q^{-1} and q^{-3} , respectively. The point q_c , where the Huang scattering transforms into the core scattering, is smaller for longer annealing. This behavior corresponds to the expected growth of precipitate sizes during the annealing. The cuts through the RSMs measured for various diffractions are plotted in Fig. 3. We can see that transition point q_c decreases with the increasing diffraction vector length and there is almost no difference between the diffuse intensity around (333) and (224) diffractions. The ratio of X-ray radii R_x determined for (333) and (111) diffractions was found to be $R_{x,333}/R_{x,111} = 1.6 \pm 0.2$ for all samples. The same value was found for the ratio of radii for (224) and (111) diffractions $R_{x,224}/R_{x,111} = 1.6 \pm 0.2$.

The simulated intensity distribution is plotted in Fig. 4(a) for the mean core radius 60 nm and deformation strength $p = 0.002$. In Fig. 4(b) we show the cuts through the map in diffractions (111) and (333) using the same input parameters. From the series of simulations for various parameters we have found out that the X-ray radius of precipitate $R_x = \pi/q_c$ corresponds to such position

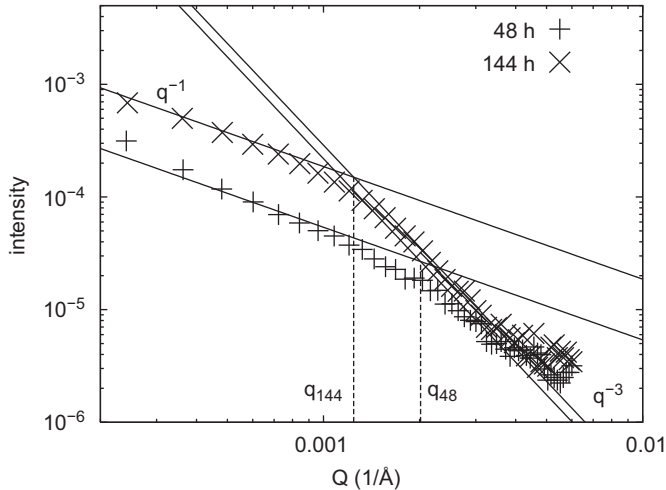


Fig. 2. The comparison of cuts through the reciprocal space maps around (111) reciprocal lattice point for the samples annealed for 48 and 144 h. The lines show asymptotic functions q^{-1} and q^{-3} for Huang and core scattering.

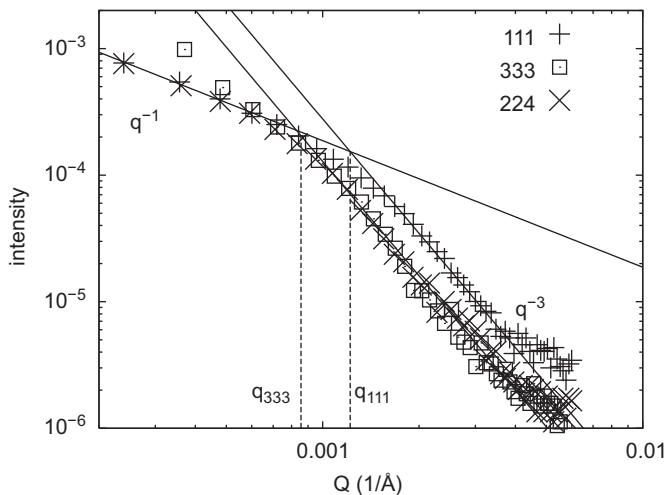
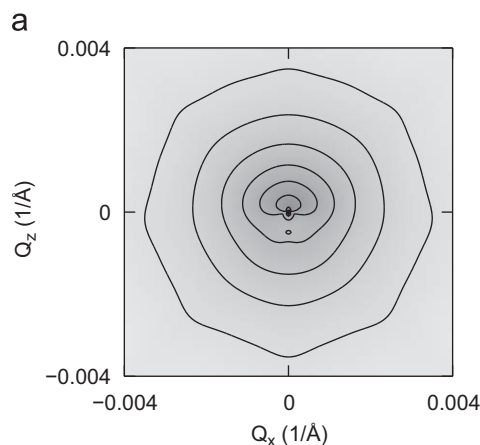


Fig. 3. The comparison of cuts through the reciprocal space maps around (111), (333) and (224) reciprocal lattice points on the sample annealed for 120 h. The lines show asymptotic functions q^{-1} and q^{-3} for Huang and core scattering. The intersection of the asymptotes are denoted as q_{111} for (111) diffraction and q_{333} for (333) diffraction, which is almost indistinguishable from (224) diffraction.



from precipitate center where $\mathbf{h} \cdot \mathbf{u}(R_x) \approx 0.1$. We ascribe this to the fact that outside this radius the approximation (5) is well satisfied and the Huang scattering decreases as q^{-1} . Closer to the precipitate the displacement is larger and the phase of scattered wave is rapidly changing. Averaging of the scattered wave intensity leads to the intensity dependence q^{-3} even from region outside of the precipitate core. Combining these results with the approximative dependence of the displacement field around the core (4), the X-ray radius has to be proportional to

$$R_x \approx \sqrt{\frac{pVh}{0.1 \cdot 4\pi}} = \sqrt{\frac{pR_c^3 h}{0.3}} \quad (6)$$

This gives the ratios of $R_{x,333}/R_{x,111} = 1.73$ and $R_{x,224}/R_{x,111} = 1.68$, which is in a good agreement with the observed values.

We have corresponded the measured X-ray radius R_x from (111) diffraction with the decrease of the interstitial oxygen ΔO_i measured by IR absorption spectroscopy, see Fig. 5. Since the precipitate concentration is the same in all samples, the decrease of the interstitial oxygen is proportional to the mean volume of SiO_2 precipitate core. If the X-ray radius R_x is proportional to the core radius, then the total volume of precipitates ΔO_i should be proportional to R_x^3 . However, we have found that ΔO_i is

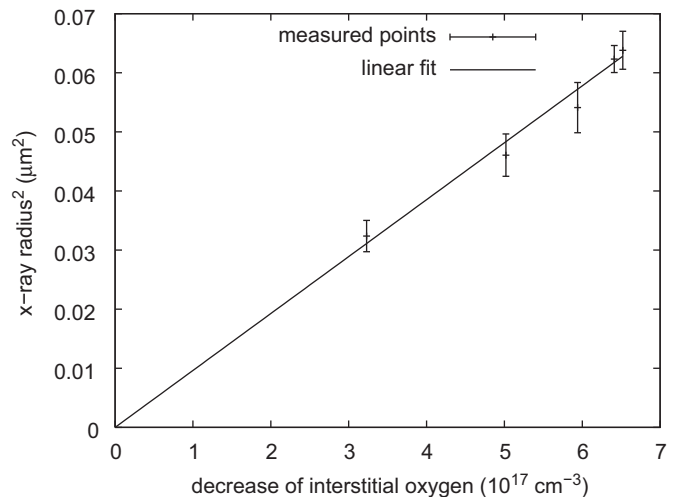


Fig. 5. The dependence of square of the X-ray precipitate radius R^2 plotted as a function of decrease of interstitial oxygen ΔO_i measured by infrared absorption spectroscopy. The line shows linear fit of the data.

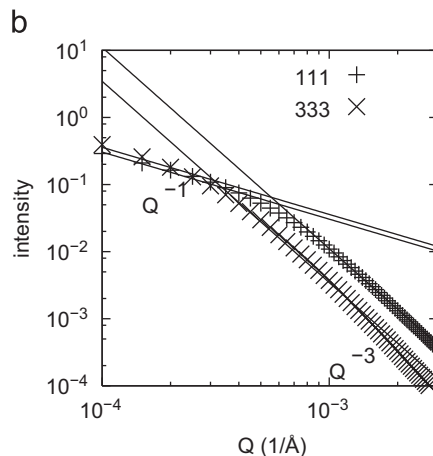


Fig. 4. Simulated reciprocal space map at (111) diffraction for spherical precipitates of mean radius 60 nm and deformation strength $p = 0.002$ (left panel). The contour step is $10^{1/2}$ and the values of Q_z -axis are counted with respect to the position of the reciprocal lattice point. The cuts through the simulated maps for (111) and (333) diffractions (right panel). The octagonal shape of the lowest contour is the artifact from the fast Fourier transform. The lines show asymptotic functions q^{-1} and q^{-3} .

proportional to R_x^2 , rather than R_x^3 , see Fig. 5. This cannot be explained by the flat shape of the precipitates, from the analysis of IR absorption spectra using method [9], we have found that most precipitates have roughly spherical shape.

However, the observed dependence of the X-ray radius R_x on the decrease of interstitial oxygen (Fig. 5) is in a good agreement with the formula (6). Assuming the precipitate concentration $3 \times 10^{11} \text{ cm}^{-3}$ we have found the precipitate deformation strength of the precipitates to be $p = 0.08$ and their core radius grows from 8 to 11 nm. If the displacement around the precipitate is smaller than $1/h$, then the approximation (5) is satisfied everywhere around the core. Only in such case, the X-ray radius $R_x = \pi/q_c$ corresponds to the precipitate core radius.

The X-ray diffuse scattering could be used to characterize precipitates of the maximum size corresponding to the coherence length of the X-ray beam. In the used experimental setup for conventional Cu X-ray tube and Bartels type Ge (220) monochromator, the coherence length is in the order of $2 \mu\text{m}$. In the case where the X-ray size of the precipitate $2R_x$ is larger than this value, one can only see the intensity of the diffuse scattering decreasing as q^{-3} and it is not possible to determine the precipitate size. The sensitivity of the method to the small precipitates is determined by the ratio of the beam to the background intensity. In our case the scattered intensity on the precipitates with X-ray radius smaller than about 100 nm is so low that the Huang-core scattering transition point is not resolvable.

5. Conclusion

We have shown that the X-ray diffuse scattering does not provide a direct information on the size of the SiO_2 particle embedded in the silicon lattice. However, in the combination with

the other experimental techniques, it can give us very important information about the strain field around the defect. We have found the interpretation of the X-ray radius R_x as the distance from the defect core where the condition $\mathbf{h} \cdot \mathbf{u}(R_x) \approx 0.1$ is valid. This interpretation corresponds very well to the experimental results measured on various diffraction orders as well as to the correspondence with IR absorption spectroscopy. The results can be generalized to the X-ray diffuse scattering on the precipitates in other materials than silicon as well.

Acknowledgments

The authors acknowledge the interest of Prof. V. Holý and the help of J. Kuběna during sample preparation. The work was part of the research project MSM0021622410 of the Ministry of Education of the Czech Republic and was supported by Czech Science Foundation projects 202/09/1013 and 202/09/P410.

References

- [1] B.C. Larson, W. Schmatz, *Phys. Stat. Sol.* (b) 99 (1980) 267.
- [2] L.A. Charnyi, K.D. Sherbachev, V.T. Bublik, *Phys. Stat. Sol.* (a) 128 (1991) 303.
- [3] P. Klang, V. Holý, J. Kuběna, R. Štoudek, J. Šik, *J. Phys. D Appl. Phys.* 38 (2005) A105.
- [4] V. Holý, U. Pietsch, T. Baumbach, *High-resolution X-ray Scattering from Thin Films and Multilayers*, Springer, Berlin, 1998.
- [5] B.C. Larson, X-ray diffuse scattering near Bragg reflections for the study of clustered defects in crystalline materials, in: R.I. Barabash, G.E. Ice, P.E.A. Turchi (Eds.), *Diffuse Scattering and the Fundamental Properties of Materials*, Momentum Press, New Jersey, 2009, pp. 139–160.
- [6] ASTM book of standards, 1996, Ch. F1188, pp. 438–441.
- [7] M.A. Krivoglaz, *X-ray and Neutron Diffraction in Nonideal Crystals*, Naukova Dumka, Kiev, 1983.
- [8] P.H. Dederichs, J. Pollman, *Z. Phys.* 255 (1972) 315.
- [9] R. Štoudek, J. Humlíček, *Physica B* 376–377 (2006) 150.